

# DETECTION OF INCIPIENT BEARING FAULTS IN A GAS TURBINE ENGINE USING INTEGRATED SIGNAL PROCESSING TECHNIQUES

Jeremy S. Sheldon  
Dr. Hyungdae Lee  
Matthew Watson  
Carl Byington, P.E.

Impact Technologies, LLC  
Rochester, NY 14623  
[carl.byington@impact-tek.com](mailto:carl.byington@impact-tek.com)

Eric Carney  
NAVAIR 4.4.2.2  
Propulsion and Power Diagnostics  
Patuxent River, MD 20670  
[eric.carney@navy.mil](mailto:eric.carney@navy.mil)

Development of a robust system for the detection of incipient bearing faults in gas turbine engines will benefit both military and civil aviation through improved aircraft reliability and maintainability. Techniques such as vibration analysis and oil debris monitoring have proven effective in laboratory and industrial settings, but several factors, including poor transmission of vibration energy from bearings to practical sensor locations, settling of debris in oil scavenge lines, and increased usage of ceramic materials, have complicated the implementation of these techniques on gas turbine engines. Presented is a gas turbine engine bearing diagnostic system that integrates information from various advanced vibration analysis techniques to achieve robust bearing health state awareness. This paper details the successful laboratory testing and implementation of the system on a gas turbine engine containing a damaged bearing, as well as the validation and verification of the system's performance using data from a ground test cell.

## Notation

*	Complex Conjugate
$a$	Scaling Parameter (or Dilation Factor)
$b$	Position Parameter
$E$	Short Time Energy
$g(t)$	Mother Wavelet
$g^{(a,b)}(t)$	Baby Wavelet
$m$	Lag
$n$	Sample Number of STE
$N$	Total Number of Samples
$N$	Data Length of $x$
$R_{xx}$	Autocorrelation Coefficients
$w$	Window Function
$x$	Discrete Signal
$x_n$	Signal
$x(t)$	Signal

## Introduction

Improving the reliability and maintainability of gas turbine engines is becoming more critical to end users concerned with reducing costs and increasing

availability. In order to reduce the cost and inconvenience of unscheduled repairs, design engineers have traditionally estimated the statistical reliability of such critical bearings and assigned a conservative safe life removal interval (based on time or usage). However, evidence has indicated that actual usage of military aircraft systems varies greatly from intended use and operating environment. Unanticipated and extreme operating scenarios are major causes of failures and unscheduled maintenance events. Actual operational lives for aircraft are commonly extended past their original design lives because of the critical mission they perform. Thus, the unfortunate reality of statistical-based preventative removals is that significant useful life remains in most units while limited failures continue to occur in the field. The former represents an opportunity to reduce maintenance time and life-cycle costs and increase readiness, while the latter represents a significant opportunity to improve safety through the implementation of diagnostic and prognostic techniques that will enable the transition from the traditional safe life removal/change intervals to condition-based approaches.

A Condition-based Maintenance (CBM) strategy promises to reduce the costs associated with scheduled maintenance by monitoring the actual condition, or

health, of the component and replacing component only when necessary and at optimally scheduled maintenance times. The authors have developed a Prognostic and Health Management (PHM) system, specifically targeting rolling element bearing health, to meet the needs of a CBM philosophy. Vibration-based features are of particular importance in determining the condition of the bearing within this system and are the focus of this paper. Analysis has shown that vibration features offer better incipient fault detection than the widely used and accepted oil debris analysis. In addition, vibration-based diagnostics offer isolation capabilities beyond oil debris monitoring.

The accuracy of bearing health predictions is critical to a robust and effective PHM implementation. Substantial research has focused on the development of robust and accurate features that can be used to increase the accuracy of health predictions; however, many of these developments have occurred in laboratory settings. Although suitable for proof-of-concept validation, the idealized laboratory test rig is often a simplified form of the target system, such as a gas turbine engine. Confounding issues, such as indirect vibration transmission path, operating condition issues, and noise sources, are often absent from the development laboratory. Complete validation of the feature or sensor is therefore possible only through actual engine tests. Therefore, the authors used data collected from an actual gas turbine engine, mounted in a full scale test cell, to validate the developed techniques. Some of the results of these tests are presented herein.

The authors focus is on engine bearings. Bearing failures are of particular concern in high performance turbines and drive trains because of the potential for catastrophic, cascading consequences throughout the system. An ability to predict early stage bearing failures will therefore affect turbine reliability and life-cycle costs both positively and dramatically.

### **Diagnostic Approach**

The developed PHM system utilizes vibration-based diagnostics, including conventional broadband features, envelope-based demodulation techniques, frequency-domain analysis, and advanced signal processing, to provide indicators of current bearing health. The incorporated envelope-based demodulation techniques utilize the high frequency impulse events generated by most early stage bearing failures [1]. Small incipient bearing faults cause these periodic impulses, which induce the modulation phenomena. Vibration amplitudes at frequencies associated with bearing faults are then extracted from the demodulated vibration spectra. These frequencies are unique to bearings and will have higher magnitudes when a fault is present.

A major technical challenge in bearing fault detection involves preventing these characteristic bearing defect frequencies from being obfuscated by surrounding mechanical and other confounding noise sources. Demodulation allows the broadband energy caused by failure effects to be differentiated from normal system noise much easier and earlier in the failure progression than traditional analysis techniques. The authors have developed an enveloping-based demodulation method called ImpactEnergy™ [2] and a demodulation scheme based on a short time energy technique to improve the detection of incipient bearing faults. Both of these demodulation methods are complimented by advanced preprocessing techniques that accentuate the modulation of the vibration signal. The following sections present descriptions of the developed diagnostic techniques that are introduced below:

- Band Selection + ImpactEnergy™ + Autocorrelation and Peak-Picking (**BIA**)
- Band Selection + Wavelet + ImpactEnergy™ + Autocorrelation and Peak-Picking (**BWIA**)
- Band Selection + Wavelet + Short Time Energy + Autocorrelation and Peak-Picking (**BWSA**)
- Band Selection + Zero-Phase Wavelet + ImpactEnergy™ + Autocorrelation and Peak-Picking (**BZIA**).

### **Band Selection**

Performance of the aforementioned demodulation techniques is dependent on the chosen frequency band. It is critical to the performance of the diagnostics to identify and use the most responsive narrow frequency bandwidths. However, identification of these frequencies is very difficult, often relying on the expertise of the vibration analyst. The authors have developed a parametric method utilizing autocorrelation and linear regression to estimate the Power Spectral Density (PSD) of a bearing vibration signal and search for any frequency ranges excited by bearing defects [3]. Figure 1 shows a time waveform of a bearing vibration signal with a ball defect and its estimated PSD superimposed on its spectrum. It is apparent there are four dominant identified frequencies, 18.8, 43.8, 50.7, and 78.2 kHz. Each of these frequencies could potentially be used to define the bandwidths for the demodulation techniques.

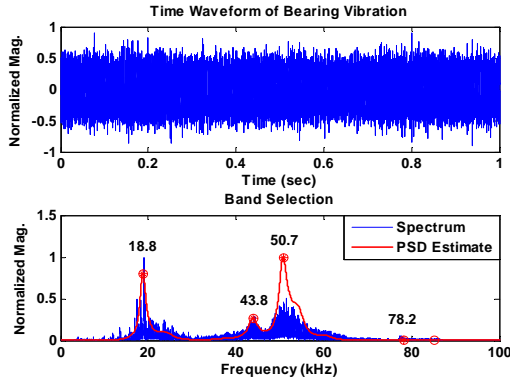


**Figure 1. Band Selection Using a Parametric Method**

### ImpactEnergy™

ImpactEnergy™ is an enveloping-based vibration feature extraction technique [2, 4] that is applied to either raw vibration data or to wavelets decomposed at pre-defined bands to obtain an envelope of the original signal. The first step in the envelope process consists of bandpass filtering the raw vibration signal. Second, the bandpass filtered signal is full wave rectified to extract the envelope. Third, the rectified signal is passed through a lowpass filter to remove the high frequency carrier signal. Finally, the signal has any DC content removed.

### Wavelet Transform

A Wavelet Transform (WT) combines the advantages of both time and frequency domain representation of a signal. The most important feature of WT is its ability to characterize the local features of the signal at different scales (i.e., frequency bandwidths). This is highly advantageous in examining the vibration signal from rotating machinery with faults, where either large-scale (caused by distributed damage) or small-scale (caused by incipient damage) changes in vibration may occur. For a signal  $x(t)$ , a Continuous Wavelet Transform (CWT) of the signal is defined as [5]:

$$W_x(a,b) = \int g^{*(a,b)}(t) x(t) dt \quad \text{Equation 1}$$

Where  $*$  denotes the complex conjugate,  $g(t)$  represents the mother wavelet, and  $g^{(a,b)}(t)$  is a baby wavelet. The mother and baby wavelets are defined by:

$$g(t) = \exp(\sigma t) \sin(\omega t) \quad t \geq 0 \quad \text{and} \quad g(t) = -g(-t) \quad t < 0,$$

$$g^{(a,b)}(t) = \frac{1}{\sqrt{a}} g\left(\frac{t-b}{a}\right) \quad \text{Equation 2}$$

Where  $a$  and  $b$  represent the scale and position at which the wavelet coefficient is calculated. The scaling parameter,  $a$ , is called the dilation factor, and the parameter  $b$  that shifts the function in time is called the translation factor. For a given  $a$ , carrying out CWT over a range of  $b$  is like passing the signal through a filter whose impulse response is defined by the baby wavelet. One may consider CWT as a bank of bandpass filters defined by a number of scales. The salient characteristic of the CWT is that the width of the passing band of the filters is frequency dependent. CWT can therefore provide a high frequency resolution at the low frequency end of the spectrum while maintaining good time localization at the high frequency end. For the developed method, a CWT with a scale corresponding to a pre-selected band is used to decompose the frequency components, which are excited by bearing defects, from the raw vibration signals. The resulting vibration signal has an enhanced signal-to-noise ratio, which will improve the results of the subsequently applied demodulation techniques.

In addition to the wavelets previously described, the authors utilize a zero phase wavelet. The Zero-Phase Wavelet is a wavelet with a Fourier transform that has zero-phase. Since the wavelet has zero-phase, the resulting wavelet transform's phase component solely depends on the phase of the signal within the passing band of the wavelet. With its ability to localize in both time and frequency domains, the magnitude component reveals local amplitude modulation and the phase component reveals local phase modulation associated with the frequency band defined by the wavelet [6].

### Short Time Energy (STE)

Short Time Energy (STE) is a demodulation technique that employs a sliding window to calculate the variation of vibration energy over time. STE can accentuate the periodic ringing due to localized defects, provided that the ringing is not completely buried in overall system noise [7]. The core of the short time energy technique is the following equation:

$$E(n) = \frac{1}{N} \sum_{m=-\infty}^{\infty} [x(m)]^2 w(n-m) \quad \text{Equation 3}$$

where  $E$  is an STE,  $n$  is a sample number of the STE,  $x$  is a discrete signal,  $N$  is the total number of samples, and  $w$  is a window function.

### Autocorrelation

Autocorrelation is the cross-correlation of a signal to itself [8]. This technique is useful for finding repeating patterns in a signal (i.e., determining the presence of a

periodic signal). Also, autocorrelation can identify a fundamental frequency of a signal that does not actually contain that fundamental frequency but only its harmonics. The discrete autocorrelation at lag ( $m$ ) for a signal  $\{x_n\}$  is defined as:

$$R_{xx}(m) = \begin{cases} \sum_{n=0}^{N-m-1} x_{n+m} x_n^* & m \geq 0 \\ R_{xx}^*(-m) & m < 0 \end{cases} \quad \text{Equation 4}$$

where  $*$  denotes the complex conjugate and  $N$  is a data length of  $x$ .  $R_{xx}$  signifies autocorrelation coefficients in a length of  $2*N-1$  vector.

When applied to bearing vibration signals, autocorrelation is used to estimate the periodicity of the demodulated signals resulting from ImpactEnergy™, WT, or STE processing. The top plot of Figure 2 is the STE of a wavelet coefficient with center frequency of 18.8 kHz, which was decomposed from the bearing vibration signal in shown in Figure 1. The bottom plot of Figure 2 shows the autocorrelation coefficients of the STE and demonstrates that the first and second peaks of the coefficients match the lines of ball defect harmonics, which is indicative of a ball defect.

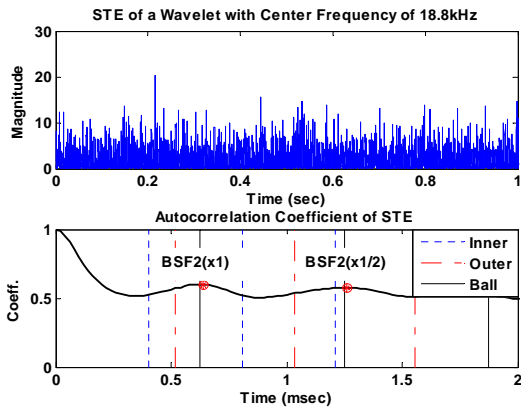


**Figure 2. Demodulation of Bearing Vibration Signal and Fault Detection**

### Test Plan

Further development and validation of the aforementioned diagnostic techniques is dependent on the availability of realistic test data. Ideally, this data would characterize several levels of bearing degradation, ranging from healthy to a severely faulted condition. Additionally, the “ideal” data would be collected from a test rig that closely simulates “in flight” testing, in order to replicate the various excitation sources and background noise.

The authors had an opportunity to collect such data from two Allison T63 gas turbine engine test rigs located at the U.S. Air Force Research Laboratory (ARFL) at Wright-Patterson Air Force Base [9]. These data collection efforts were greatly supported by the University of Dayton Research Institute (UDRI) and AFRL. Although located in a test cell, the Allison engine test rig closely replicated the engine conditions (speeds, temperatures, and loads) experienced during flight. Three charge-type accelerometers were used to acquire the vibration signature of the engine. The first accelerometer was radially stud-mounted near the compressor inlet. The second accelerometer was radially affixed to the top lift point and the third accelerometer was axially attached to the main engine gearbox. The accelerometer signals were sampled with commercially available hardware.

In order to characterize the various bearing damage levels in the engine, tests were performed with three different bearings. All bearings tested were gas generator shaft (engine) bearings, from the second (aft) bearing location. First, a healthy bearing with no faults was used to generate baseline data. Second, a bearing with a seeded inner raceway fault was used to generate incipient fault data. The fault on the second bearing was seeded by placing two dents (Brinell marks) in the anticipated load path of the bearing (see Figure 3). The intent of the marks was to cause the initiation and progression of a spall during testing to characterize fault progression. The third bearing used in testing had a large, pre-existing spall on the inner raceway and was used to generate data representative of a severe fault.



**Figure 3. Dented Inner Raceway, SEM**

In order to replicate the conditions that the engine might experience during flight, a modified flight profile (shown in Figure 4) was used throughout the testing. Rather than a single, long test run, each test was segmented into several test runs (cycles). Each test cycle followed a speed profile consisting of three gas generator speed levels: military power, cruise power, and idle power. Each test cycle was approximately 35

minutes long and consisted of three excursions to military power (2 minutes each) with cruise power for 5 minutes between excursions and idle power in between profiles.

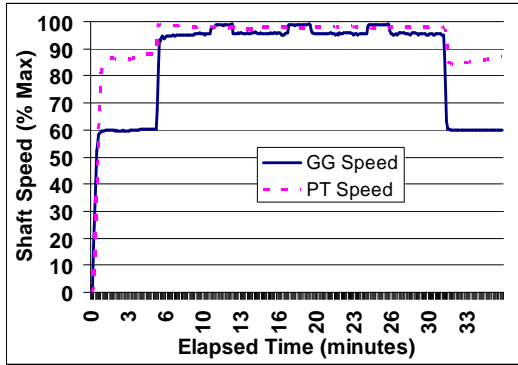


Figure 4. T63 Test Profile

### Test Results

For each bearing condition, multiple test cycles were performed. Two cycles were run on the healthy bearing, which translated to approximately 1 hour of test time. Sixty-six cycles were run on the dented bearing, which translated to approximately 43 hours of test time. Four cycles, approximately 2 hours, were run on the prespalled bearing. Test time on the spalled bearing was limited due to concerns about the rapid spall progression. More cycles were put on the dented bearing to initiate, and hopefully propagate, the dent into a spall. Each of the aforementioned diagnostic techniques was then applied to the collected data.

Successful diagnostic features need the ability to detect an anomaly in the monitored system with minimal false alarms, isolate potentially faulted components, and provide useable correlations to system health [10]. The following sections detail the diagnostic capabilities of the various developed techniques. Results presented are from a single accelerometer location (gearbox) and only from the high speed and load condition (military power). This is because the gearbox accelerometer provided the clearest indication of the fault. In addition, the feature magnitudes varied the least during military power, resulting in more robust diagnostic features. Also, the signal's modulation was more pronounced during military power than during the other regimes.

To establish ground truth, the raceways were visually inspected twice during and once after the testing was complete. Upon final inspection of the dented raceway, spall initiation and slight progression was witnessed (see Figure 5 as compared to Figure 3). Although the spall had progressed, it was still a very small, incipient fault. Please note that the results shown here are from

only during military power, which the engine was run at for 375 minutes (the total run time was 2400 minutes). The feature trend shown in the following figures is divided into stages to investigate the shifts in feature distribution as the test progressed. The stages correspond to intermediate teardown inspections of the engine to document the fault progression.

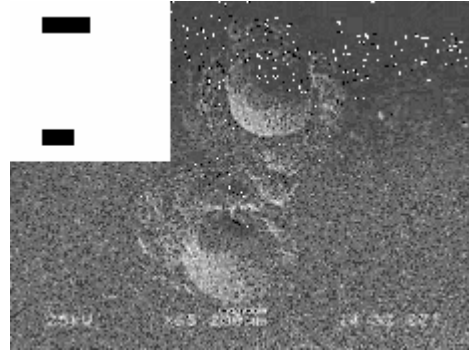
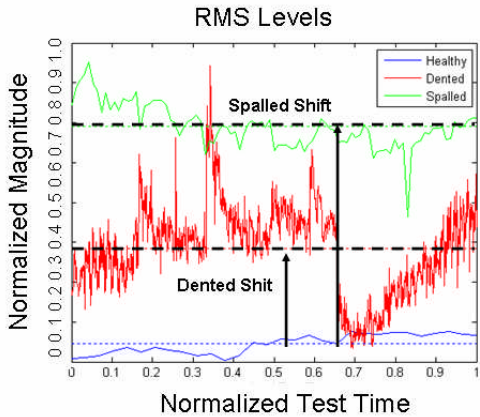


Figure 5. Dented Raceway End of Testing, SEM

### Anomaly Detection

A feature's anomaly detection capability is simply its response to some change in the monitored system's health state. In other words, an anomaly feature indicates only that a change has taken place; it does not indicate what has changed. While sometimes sensitive to operational conditions, these types of features are generally only useful when compared against similar operational regimes. The robustness of an anomaly feature is measured by its sensitivity to system changes. One measure of this sensitivity is the feature's magnitude change under varying system health conditions. This value shift leads to a separation of the healthy values from the unhealthy values. Figure 6 shows the normalized RMS values calculated during the military operating conditions for all three test cases. The military operating regime induces the highest loads on the bearing, which generates stronger vibration, resulting in a greater separation of the features between bearing conditions. The RMS magnitudes for each bearing case are shown versus a normalized test time (since each test ran had a different duration). The means for each case are also shown as dashed lines.



**Figure 6. RMS Magnitudes at the Military Operating Condition**

Figure 7 shows the Probability Density Functions (PDFs) for each test case, assuming lognormal distributions. This plot clearly shows the separation between the three bearing conditions. It is worth noting that many other features were also calculated, but only RMS is presented for brevity.

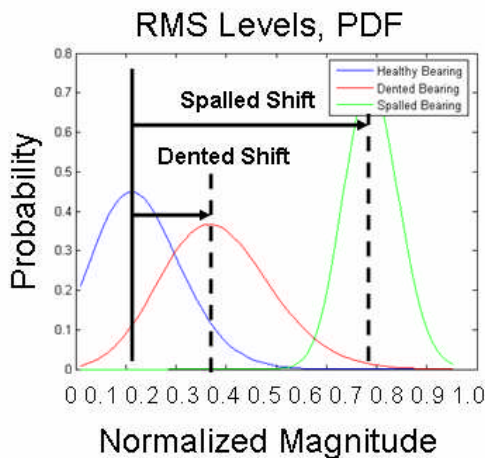


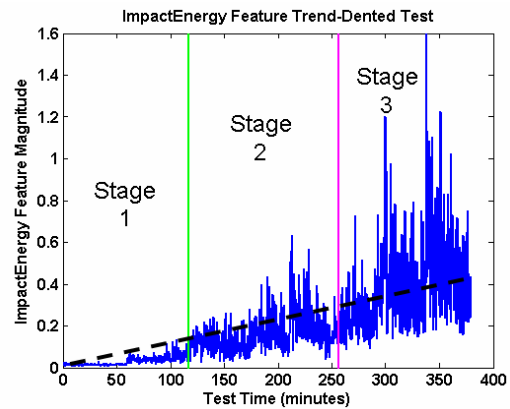
**Figure 7. Normalized RMS PDFs at Military Operating Condition**

### Diagnostic Technique Comparison

The diagnostic methods defined previously were applied to the vibration data collected during the healthy and dented bearing tests. Features were also trended over time to investigate the features' correlation to spall progression, and therefore bearing health. Reliable feature/component health correlation allows thresholds to be set based on acceptable damage tolerances. The final PHM prediction is also more accurate and robust when the system incorporates a reliable, damage-correlated diagnostic feature. That is, the resultant final health indicator generated by the PHM system will more accurately trend the actual bearing health when features are incorporated that correspond with the existing

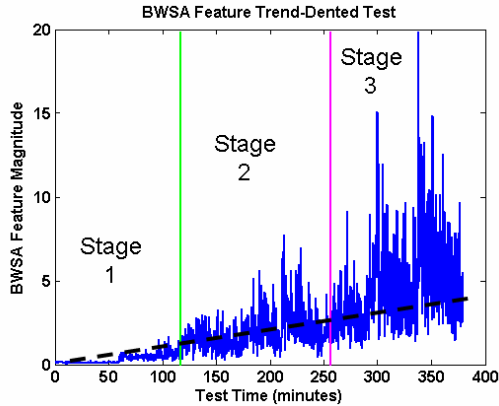
damage. In order to accurately compare the various techniques, the same (automatically selected) narrow band frequencies were used in each technique.

Figure 8 shows a BIA feature's trend over the duration of the dented bearing test. As previously noted, a tear down inspection was performed at the end of each "Stage" to determine ground truth. As seen, fluctuations exist due to variations in speeds and loads. These fluctuations are expected, since feature magnitude is strongly dependent upon operating condition. However, there is a gradual increase in the trend that correlates well with the progression of the fault. This feature response is significant and promotes prognostic capability for fault progression prediction and remaining life estimates.



**Figure 8. Dented Raceway BIA Feature Trend**

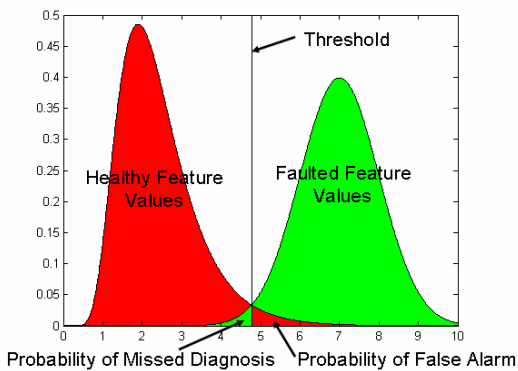
Figure 9 show a BWSA feature's trend. Again, the trend is divided into stages to promote analysis of the statistical shift. The trend closely resembles the BIA trend because they both are demodulation-based techniques that use similar narrowband filters. However, the magnitudes of the BWSA feature are greater than the BIA features, which is important in the separation of healthy and faulty features. The other techniques showed similar feature trends, and are therefore not presented.



**Figure 9. Dented Raceway BWSA Feature Trend**

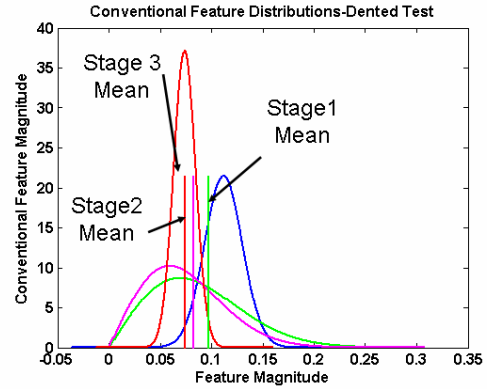
### Statistical Separability

Statistical separation of features is critical to any diagnostic system's performance. Diagnostics must be able to sufficiently distinguish between healthy and faulted features, and therefore, health states. Two commonly used measures of feature performance are the missed detection and false alarm rates. The missed detection rate is related to the probability that a feature value from a faulted bearing will not exceed a threshold when it should, thus resulting in the missed detection of a failure. The false alarm rate is related to the probability that a feature value from a healthy bearing will exceed a threshold, thus resulting in a false indication of a failure. Figure 10 illustrates the statistical feature analysis. This analysis is important in selecting the optimal diagnostic technique to maximize correct detection while minimizing false alarms [11].



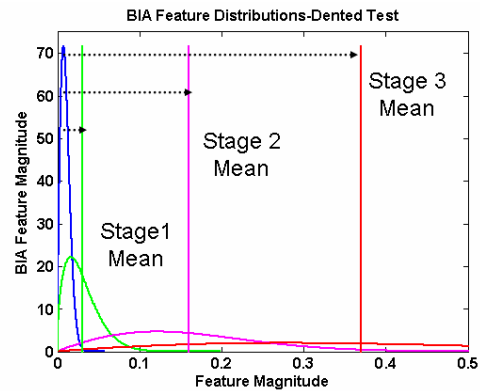
**Figure 10. Statistical Feature Analysis**

This statistical analysis was first conducted on a conventional bearing feature for comparison, as seen in Figure 11. The feature is the magnitude of the inner raceway defect frequency calculated from the raw vibration spectrum. Clearly, there is no reliable shift in the frequency magnitude and this feature could not be used for detecting the fault at any stage of progression.



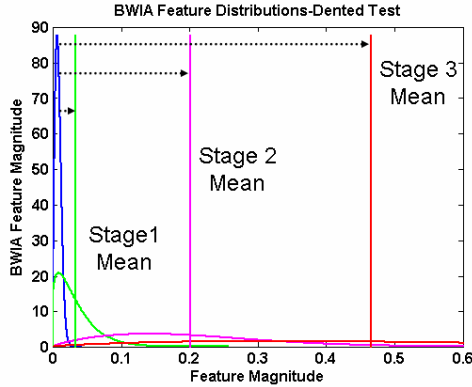
**Figure 11. Conventional Feature Separation**

Figure 12 shows the feature separability of the BIA technique. The healthy feature distribution is compared to the means of the dented features from the three stages of data. The plot in Figure 12 clearly shows the shifting feature distribution as the fault progresses. As the damage from the spalled dent increases, the distributions become further separated.



**Figure 12. BIA Feature Separation**

As seen in Figure 13, the BWIA technique provides better separation than the BIA technique. The Stage 1 mean is out on the tail of the healthy distribution and the Stage 3 mean is farthest to the right.



**Figure 13. BWIA Feature Separation**

As seen in Figure 14, the BWSA technique also performed well and has similar characteristics to the BWIA.

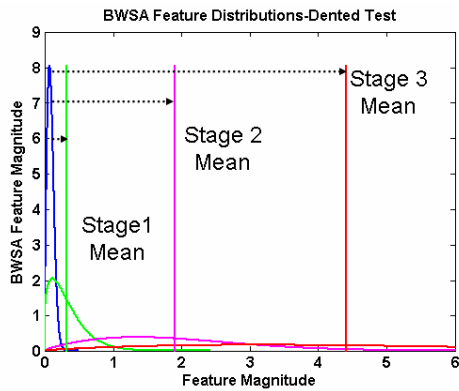


**Figure 14. BWSA Feature Separation**

Figure 15 shows the separation resulting from the BZIA technique. Notice that the Stage 1 mean of the BZIA technique is actually still well within the healthy distribution. This is an indication that the BZIA technique may not perform as well as the other techniques because it provides less feature separation.

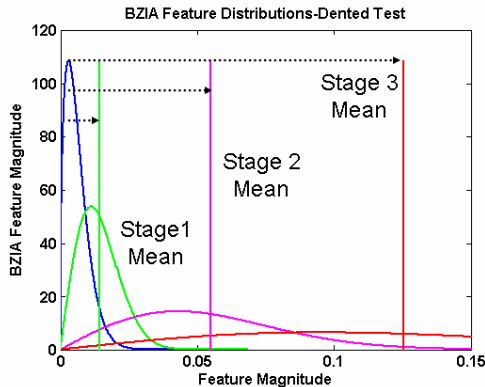


**Figure 15. BZIA Feature Separation**

In order to compare the detection abilities of the various techniques, the missed detection rates were calculated for each. This was performed by defining a threshold that results in an acceptable false alarm rate and then evaluating the resulting missed detection rate. For this evaluation, a 2% false alarm rate was used for each stage and each technique. The results of the missed detection rate analysis are detailed in Table 1. As seen, the BWIA technique slightly outperforms the rest of the techniques, since it shows a lower missed detection rate at every stage.

**Table 1. Missed Detection Rate Analysis**

Method	Threshold	Miss Detection Rate (%)		
		Stage 1	Stage 2	Stage 3
Conv	0.149	90	96	100
BIA	0.024	45	2.3	0.5
BWIA	0.019	38	1.4	0.3
BWSA	0.216	39	1.7	0.4
BZIA	0.018	70	8.3	1.7

Although, the conventional approach did not perform well at any stage of fault progression, the four developed approaches performed much better. As seen, the Stage 1 detection capability of all four developed approaches was better but still relatively low, with the BZIA approach performing the worst. However, all four approaches performed well at Stage 2 and State 3 of the fault progression, with each achieving a P(MD) less than 2%. These results are impressive when considering that the Stage 3 fault was still relatively small and could be considered incipient. The detection capability of all four methods is therefore impressive, and the Stage 1 detection performance of the BWIA and BWSA is even more impressive. These metrics allow a PHM system designer to quantify the performance of potential diagnostics. In this instance, the BWIA and BWSA approaches performed better than the other techniques during each stage.

## Conclusions

As part of this work, conventional and new signal processing techniques were combined in different ways to detect bearing faults. These methods were applied to data collected from baseline and seeded fault bearing tests to verify the efficacy of the integrated techniques. The developed diagnostic features were proven effective in detecting incipient bearing faults. The presented features meet the requirements of successful PHM diagnostic features. First, the features provide sufficient separability to be useful in fault detection, providing an impressive level of detection horizon. Second, they provide a reliable correlation with component health, enabling prognostics and remaining life prediction. Finally, they meet commonly used PHM system

benchmarks. As expected, the confounding vibration sources experienced on the engine greatly increased the difficulty in detecting incipient faults and reduced some of the feature effectiveness. However, the use of test data with confounding vibration sources provides a more realistic indication of how these techniques will perform in engine applications.

It is concluded that bearing fault detection is highly affected by the hybrid diagnostic techniques that are implemented, as well as the bandwidths chosen for scrutiny. In other words, the proper selection of the vibration bands and diagnostic techniques will result in better estimation of bearing health. In general, none of the four techniques considered here outperformed the others, but the BWIA and BWSA techniques were slightly more sensitive to incipient fault detection. In addition, all four approaches significantly outperformed traditional bearing fault detection approaches. Therefore, each of the techniques documented in this paper needs to be used in conjunction with the others to maximize the accuracy of fault detection, classification, and trending of bearing health degradation.

#### Acknowledgments

This work has significantly benefited from the support and technical consult of Michael Begin, Andy Hess, and Michael Thorsen of the Naval Air Warfare Center (NAVAIR) and Joint Strike Fighter program office. Also, the authors would like to give a special thanks to Chris Klenke, Matthew Wagner, Ken Semega, and Nelson Forrester of the Air Force Research Laboratory (AFRL), all of whom have provided invaluable advice and assistance to the developed work. The financial support for this work, provided by the NAVAIR and Air Force Small Business Innovative Research (SBIR) to program office through multiple contracts (Contract numbers N68335-05-C-0196 and F33615-03-C-2364), is also gratefully acknowledged.

#### References

1. D'Amato, E., and Rissone, P., "Using the Envelope Method to Monitor Rolling Bearings," Proc. 1<sup>st</sup> Intl. Mach. Monitoring Diagnostic Conf., Las Vegas, NV, Sept. 11-14, 1998, pp. 560-566.
2. Orsagh, R., Roemer, M., and Klenke, C., "Fusion-Based Prognostics/Diagnostics For Oil-Wetted Components In Gas Turbines Engines," 56<sup>th</sup> Meeting of the Society for Machinery Failure Prevention Technology (MFPT), Virginia Beach, VA, April 2002, pp. 67-79.
3. Stoica, P., and R.L. Moses, Introduction to Spectral Analysis, Prentice-Hall, 1997.
4. Orsagh, R.F., Sheldon, J., and C.J. Klenke, "Prognostics/Diagnostics for Gas Turbine Engine Bearings," Proc. STLE Annual Meeting, New York, NY, April 2003.
5. Wang, C., and R. Gao, "Wavelet Transform with Spectral Post Processing for Enhanced Feature Extraction," IEEE Trans., Instrum. Meas., Vol. 52, (4), Aug. 2003.
6. Li, C.J., "Zero Phase Wavelet Transform for Detecting Bearing Localized Defects," Proc. 59<sup>th</sup> Meeting of the Society for Machinery Failure Prevention Technology (MFPT), Virginia Beach, VA, April 18-21, 2005.
7. Li, C.J., and S.M. Wu, "On-line Detection of Localized Defects in Bearings by Pattern Recognition Analysis," ASME J. of Engineering for Industry, Vol. 111, (4), Nov. 1989, pp. 331-336.
8. Orfanidis, S.J., Optimum Signal Processing - An Introduction, 2<sup>nd</sup> ed., Prentice-Hall, Englewood Cliffs, NJ, 1996.
9. Klenke C., Saba C., and Toth, D., "Minisimulator for Evaluating High-Temperature Candidate Lubricants: Part I: Method Development," Tribology Transactions, Vol. 44, (2), 2001, pp. 277-283.
10. Byington, C., Roemer, M., Kalgren, P., and Vachtsevanos, G., (2005), "Verification and Validation of Diagnostic/Prognostic Algorithms," Proc. 59<sup>th</sup> Meeting of the Society for Machinery Failure Prevention Technology (MFPT), Virginia Beach, VA, April 18-21, 2005.
11. Smith, M., Byington, C., Kalgren, P., Parulekar, A., and DeChristopher, M., "Layered Classification for Improved Diagnostic Isolation in Drivetrain Components," IEEE Aerospace Conference, Big Sky, MT, March 4-11 2006.
12. Orsagh, R., Lee, H., Watson, M., Byington, C., and Powers, J., (2005), "Application of Health and Usage Monitoring System (HUMS) Technologies to Wind Turbine Drive Trains," WindPower 2005, Denver, CO, May 15-18, 2005.
13. Pattada, K., Byington, C., Kalgren, P., and DeChristopher, M., (2005), "High Frequency Incipient Fault Detection for Engine Bearing Components," ASME Turbo Expo 2005: Power for Land, Sea and Air, Reno-Tahoe, NV, June 6-9, 2005, Paper Number: GT2005-68516.
14. Kalgren, P., Byington, C., Pattada, K., and Riazzi, R., "Bearing Incipient Fault Detection Technical Approach, Experience, and Issues," 59<sup>th</sup> Meeting of the Society for Machinery Failure Prevention Technology (MFPT), Virginia Beach, VA, April 18-21, 2005.